ADVANCES IN ATMOSPHERIC SCIENCES, VOL. 22, NO. 4, 2005, 496–508

Climatology and Variability of the Indonesian Throughflow in an Eddy-permitting Oceanic GCM

LIU Hailong* (刘海龙), LI Wei (李 薇), and ZHANG Xuehong (张学洪)

State Key Laboratory of Numerical Modeling for Atmospheric Sciences and Geophysical Fluid Dynamics (*LASG*), *Institute of Atmospheric Physics, Chinese Academy of Sciences, Beijing* 100029

(Received 3 December 2004; revised 18 March 2005)

ABSTRACT

A quasi-global eddy permitting oceanic GCM, LICOM1.0, is run with the forcing of ERA40 daily wind stress from 1958 to 2001. The modelled Indonesian Throughflow (ITF) is reasonable in the aspects of both its water source and major pathways. Compared with the observation, the simulated annual mean and seasonal cycle of the ITF transport are fairly realistic. The interannual variation of the tropical Pacific Ocean plays a more important role in the interannual variability of the ITF transport. The relationship between the ITF and the Indian Ocean Dipole (IOD) also reflects the influence of ENSO. However, the relationship between the ITF transport and the interannual anomalies in the Pacific and Indian Oceans vary with time. During some years, (e.g., 1994), the effect of a strong IOD on the ITF transport is more than that from ENSO.

Key words: Indonesian throughflow, eddy-permitting oceanic GCM, the interannual variability

1. Introduction

It has been documented by a number of observations that there exist significant mass and heat transports from the Pacific to the Indian Ocean by the Indonesian Throughflow (ITF) [see the reviews of Godfrey (1996) and Gordon (2001)]. Numerical simulations based on both the stand-alone oceanic general circulation models (GCMs) and the coupled ocean-atmosphere GCMs have also shown evidence of the relationship between the variation of ITF and ocean circulation and global climate (Hirst and Godfrey, 1993; Schneider, 1998; etc.). Thus it is desirable to quantify not only the climatology but also the variability in the long term of the ITF transport.

Due to insufficient observations, model studies play an important role in ITF investigations. By means of a numerical model, a fine grid is needed to resolve the complicated bathymetry within the Indonesian Seas. With grid sizes approaching the ability to resolve eddies, some global oceanic GCMs have been applied to simulate the ITF transport and the circulation within the Indonesian Seas. As a result of the inaccurateness of the individual models and the differences between models (resolution, physical processes, forcing fields), the simulated ITF transport varied over a large range. For instance, the annual mean transport was 7.4 Sv (1 Sv=10^6 m^3 s^{-1}) according to Potemra et al. (1997), 4–12 Sv in Gordon and McClean (1999), and approximately 20 Sv in Fang et al. (2003). It is recognized that a high resolution and realistic forcing fields are critical for a successful model study of ITF.

The ITF tends to have a small transport during El Niño and a large transport during La Niña (Clarke and Liu, 1994; Meyers, 1996; Ffield et al., 2000), suggesting an important climate implication of the ITF and prompting particular interest in study of the ITF. Based on the observed temperature along line IX1 (Fig. 1), and climatological temperature-salinity relations, Meyers (1996) found two leading empirical orthogonal function (EOF) modes of the ITF transport across its Indian Ocean entrance. The first one was an ENSO (El Niño-Southern Oscillation) pattern whereas the second came from the equatorial Indian Ocean, indicating that the interannual variability of the ITF transport has a relationship with both the Pacific and Indian Oceans. The existing model studies, however, paid more attention to the connection between the interannual variability of the ITF and ENSO (Potemra et al., 1997; Gordon and McClean, 1999; Liu, 2002).

*E-mail: lhl@lasg.iap.ac.cn

In the present study, a quasi-global, eddy-permitting oceanic GCM is driven by observed wind to yield the time series of ITF transport for 1958–2001. Details of the model and experiments are described in section 2. The modeled climatology of the annual mean and seasonal cycle of the Indonesian Seas circulation are shown in section 3. The climatology and interannual variability of the ITF transport are presented and compared with the available observations in sections 4 and 5, respectively. The relationship between ITF, ENSO, and the interannual signal in the Indian Ocean is also investigated in section 5. A summary is given in section 6.

2. Model and experiment

The LASG/IAP (State Key Laboratory of Numerical Modeling for Atmospheric Sciences and Geophysical Fluid Dynamics/Institute of Atmospheric Physics) Climate System Ocean Model (version 1.0; abbreviated as "LICOM1.0"; Zhang et al., 2003; Liu et al., 2004a, 2004b) has been newly developed based on the third generation of the oceanic GCM of LASG/IAP, namely L30T63 (Jin et al., 1999). LICOM1.0 has the same dynamical and computational frameworks as L30T63. Some mature physical parameterization schemes, including the isopycnal mixing scheme (Gent and McWilliams, 1990), the Richardson-number-dependent vertical mixing in the tropical oceans (Pacanowski and Philander, 1981), were inherited from L30T63.

LICOM1.0 is quasi-global (75°S–65°N) with a horizontal resolution of a uniform 0.5° by 0.5° grid, which is its major improvement over L30T63 (resolution of about 1.875° by 1.875°. There are totally 30 levels in the vertical with 12 levels for the upper 300 m. Additionally, the application of a Message Passing Interface (MPI) in the parallel computation makes it possible for a long-term integration. See Liu et al. (2004a) for more details about LICOM1.0.

The model bathymetry was derived from DBDB5 (Digital Bathymetric Data Base 5 minute) dataset produced by the Naval Oceanographic Office, USA. The main pathways of the ITF in the Indonesian Seas, including the Makassar, Maluku, Halmahera, Lombok,

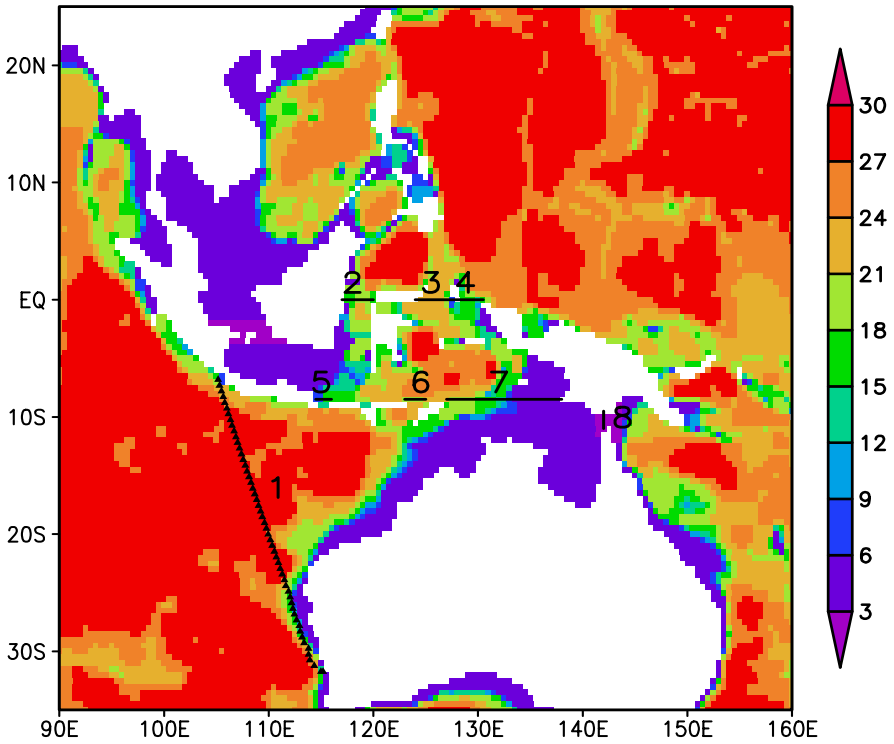

Fig. 1. The topography of LICOM1.0 in the vicinity of the Indonesian Sea. The coloring marks the amount of levels. The numbered lines denote sections along which the transports are calculated. 1: line IX1, 2: Makassar Strait, 3: Maluku Strait, 4: Halmahera Sea, 5: Lombok Strait, 6: Ombai Strait, 7: Timor Passage, 8: Torres Strait.

and Ombai Straits and the Timor Passage etc., can be explicitly represented in the model (Fig. 1). Some extra alterations were made by hand to improve the representation of major ridges and sills.

A 900-year spin-up run was conducted from the initially motionless ocean and the temperature and salinity fields of Levitus and Boyer (1994) and Levitus et al. (1994). The model was integrated synchronously with time steps of 60 s, 1800 s, and 3600 s for the barotropic, baroclinic, and temperature and salinity integrations, respectively. A Laplacian-type viscosity scheme is applied with coefficients of 2.0×10^3 m^2 s^{-1} between 50°S and 50°N and 2.0×10^5 m^2 s^{-1} for the poleward regions.

A formula with a flux correction term is adopted for the sea surface heat forcing. This method is based on the pioneer work of Haney (1971). The underlying idea is to express the feedback to the atmosphere as a flux correction which depends upon the model SST. The method can overcome the physical inconsistency due to the lack of air-sea feedbacks in the formulation of the atmospheric forcing of ocean models. The formula is as follows:

$$Q_{\text{net}} = Q_{\text{solar}} + Q_{\text{non-solar}} - \frac{\partial Q_{\text{non-solar}}}{\partial T_{\text{ss}}} \times (T_{\text{ss, model}} - T_{\text{ss, obs}}) , \quad (1)$$

where Q_{net}, Q_{solar} and $Q_{\text{non-solar}}$ represent the total net heat flux, the solar radiation and the heat flux without the solar radiation, respectively. The third term on the right hand side stands for the flux correction term. The coefficient $\partial Q_{\text{non-solar}}/\partial T_{\text{ss}}$ is the "dumping coefficient". $T_{\text{ss, model}}$ and $T_{\text{ss, obs}}$ are the SSTs predicted by LICOM and the observed, respectively. The later is from *World Ocean Atlas 1998* (National Oceanographic Data Center, 2004). The Q_{solar} and $Q_{\text{non-solar}}$, as well as the dumping coefficient, are all from the OMIP-Forcing datasets (Roeske, 2001), which is a climatological dataset for forcing global ocean models derived from the European Centre for Medium-Range Weather Forecasts re-analysis (ERA15, Gibson et al., 1997). The mean annual cycle has been produced from the 15 years of ERA by using Gaussian filtering with daily fluctuations superimposed. The budgets of the heat and the fresh water fluxes have been closed by modifying the bulk formulae.The sea surface salinity (SSS) was simply restored to the observational monthly climatology of WOA98. The wind stresses are also from the OMIP-Forcing datasets (Roeske, 2001).

The performance in terms of the climatology of the large scale circulation, distribution of upper temperature and permanent thermocline, and oceanic meridional heat transport of the LICOM1.0 spin-up run has been evaluated by Liu et al. (2004b), in which remarkable improvements in many aspects against L30T63 were found, especially in the tropical circulation.

After the spin-up run, a 44-year (1958–2001) experiment was driven by ERA40 daily wind stresses (ECMWF Re-Analysis 40, http://www.ecmwf.int/research/era/). The heat and freshwater surface conditions are kept by restoring them to the observational climatology as in the spin-up run. All the analyses are based on the monthly output of the last 44-year integration.

3. Circulations in the Indonesian seas

3.1 *Annual mean climatology*

It is confirmed by the properties of water mass that the main body of the model ITF traces back to the thermocline and intermediate layer of the North Pacific. It flows into the Sulawesi Sea via the Mindanao Current (MC) and enters the Indonesian Seas through the Makassar Strait (Gordon and Fine, 1996). There is also a small quantity of water from the South Pacific invading the Indonesian Seas through the deep passages to the east of Sulawesi (Gordon and Fine, 1996).

At the surface and in the thermocline of LICOM1.0 (Figs. 2a, b), the simulated ITF comes straight from the Mindanao Eddy (ME) and the Halmahera Eddy (HE) located between the Philippines and New Guinea. A portion of water from the ME enters the Indonesian Seas through the Makassar Strait while the rest turns eastward to feed both the North Equatorial Countercurrent (NECC) and the Equatorial Undercurrent (EUC). Due to the presence of Halmahera Island, most of the South Pacific upper water flows clockwise around the HE and retroflects to merge with the eastward current from the MC. A small quantity of South Pacific water enters the Seram Sea and divides into two branches. The northward branch returns to the Pacific and the southward one flows into the Banda Sea. Besides this, there are also fewer water exchanges through the Torres Strait (between New Guinea and Australia) and the Karimata Strait (southern end of the South China Sea). The outflow of the Indonesian Seas is mainly through the Ombai and Lombok Straits, though the latter is shallow in depth. Murray and Arief (1988) found only an average southward transport of 1.7±1.2 Sv in the Lombok Strait. The error is also addressed by others, such as Masumoto and Yamagata (1996) and Potemra et al. (1999). Shiller et al. (1998) suggested that increasing the meridional eddy viscosity in the Lombok Strait will block the transport through the Lombok Strait and alleviate the er-

ror. There is also a fraction of water that enters the Indian Ocean by the Timor Passage.

Below the thermocline (Figs. 2c, d), water exchange between the Pacific and Indian Oceans can only occur via the eastern channels. The water from the MC flows straight into the Banda Sea through the Maluku Strait because the Taliabu and Mangole islands are absent in the model topography and it enters the Indian Ocean through the Ombai Strait and Timor Passage. At 300 m, the South Pacific water flows along the eastern coast of New Guinea and turns eastward without entering the Indonesian Seas when it reaches the equator. At a deeper layer of about 800 m, it is clear that some South Pacific water enters the Indonesian Seas.

The salinity stratification in the Indonesian Seas further corroborate the water source of the ITF. Figure 3 gives the sections of the salinity for the upper 500 m within the two primary passages of the ITF. In the Makassar Strait, the subsurface salinity maximum (around 100 m) and minimum (around 300 m) denote the presence of North Pacific thermohaline water (NPTW) and North Pacific intermediate water (NPIW), respectively. Both water masses extend southward, being coincident with the circulation pattern presented in Fig. 2. The distribution of North Pacific water masses in the Makassar Strait agrees well with the Arlindo observational data (Gordon and Susanto, 1999), which also implies a realistic circulation in LICOM1.0. The saltier NPTW and fresher NPIW in the model may be caused by the absence of tidal mixing, which is of significance for the thermal or salinity stratification in the Indonesian Seas (Ffield and Gordon, 1992; Schiller et al., 1998).

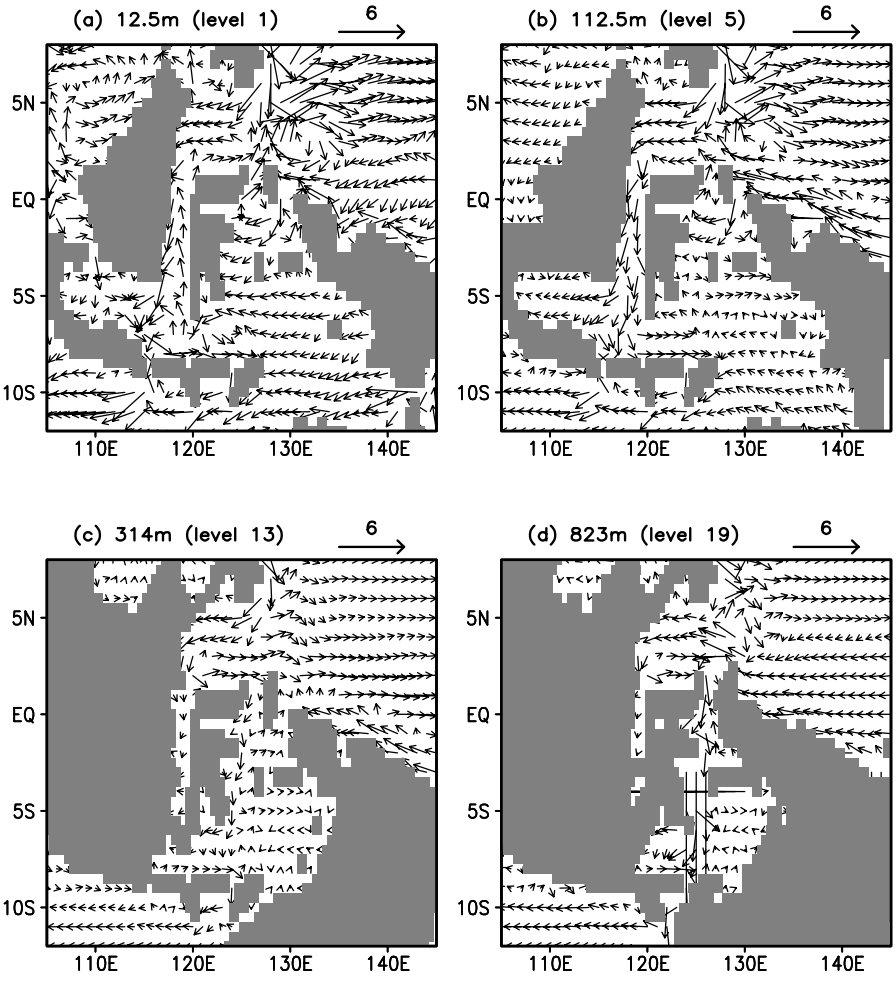

Fig. 2. The simulated annual mean circulations at (a) 12.5 m, (b) 112.5 m, (c) 314 m and (d) 823 m within the Indonesian Seas in LICOM1.0. The currents have been divided by the square root of the scalar speed. Units: $m^{1/2}\ s^{-1/2}$.

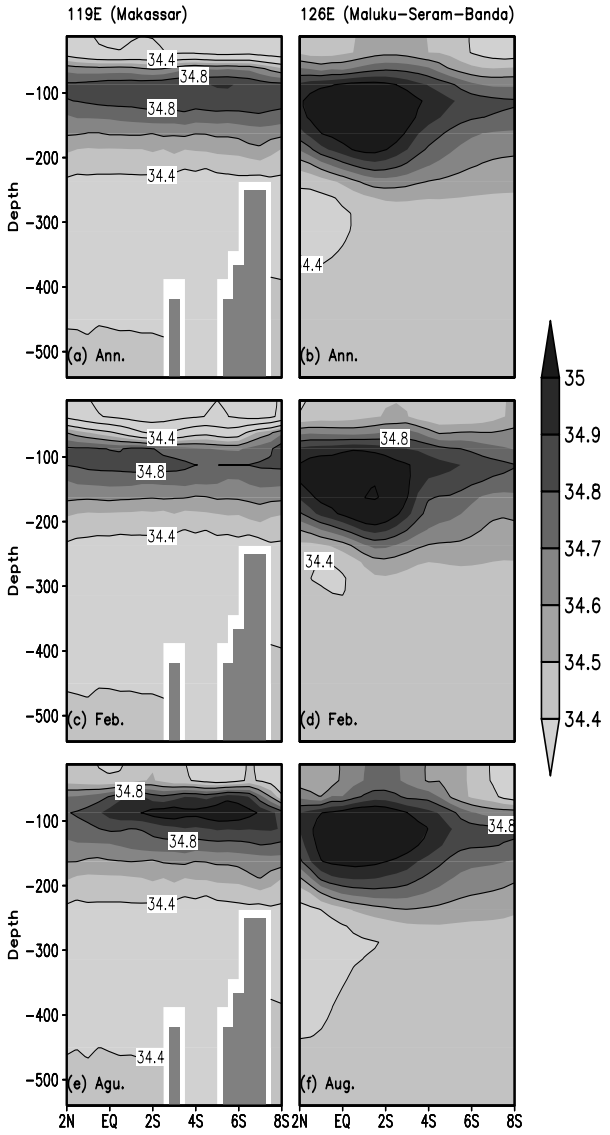

Fig. 3. Sections of simulated salinity for the upper 500 m within the Makassar Strait (119°E) (a, c, e) and from the Maluku Strait to the Banda Sea (126°E) (b, d, f). (a) and (b) are for annual mean, (c) and (d) for February, (e) and (f) for August. Units: psu.

It was shown in the Arlindo observations that the North Pacific water is only present at the entrance of the Maluku Strait. To the north of the Banda Sea, there is a salinity maximum at about 500 m which denotes its water source as the South Pacific (Gordon and McClean, 1999). While the depth of the Halmahera Sill (about 540 m) is realistic in LICOM1.0, the width of only one row of velocity grids in the deep layers is too narrow. As a result, the South Pacific water intrusion in the deep layers is limited. Instead, a salinity maximum is present at about 150 m (Fig. 3b), consistent with the circulation in Fig. 2b where the South-Pacific-sourced water is evident. The water from the North Pacific is dominant below the thermocline, a feature that can also be found in Fig. 2c. This problem of the narrow deep channel of the Halmahera Sill was also encountered by Godfrey and Masumoto (1999).

3.2 *Seasonal cycle*

Due to the reversal of the Asian-Australian monsoon, the surface circulation is characterized by strong seasonal variation in the Indonesian Seas. The surface currents in the Banda Sea accord with the prevailing winds: eastward in boreal winter and westward in boreal summer (Figs. 4a, c). The Ekman transport of boreal winter monsoon blocks the transport from the Pacific to the Indian Ocean. The surface currents in both the Makassar Strait and channels east of Sulawesi head northward and there are transports from the Indian Ocean to the Indonesian Seas via the Ombai Strait and Timor Passage. The summer monsoon, on the other hand, favors the transport from the Pacific to the Indian Ocean. The currents within the Indonesian Seas are almost opposite to those during the winter except for the Lombok Strait, i.e., southward all year round. The directions of the currents in the main straits, such as the Makassar Strait, the Maluku Strait, the Halmahera Strait etc., are almost the same as the surface currents observed by Wyrtki (1961) both in February and August.

The salinity in the Maluku Strait is high in the boreal winter and low in the boreal summer at the surface (Figs. 3d, e), which is mainly caused by the seasonal variations of local precipitation and the Sulawesi runoff.

In the thermocline, the current within the Makassar Strait remains southward all year long (Figs. 4b, d) with a larger transport during the boreal summer. The seasonal variations of the currents are also clearly reflected in the charts of salinity. Comparison between Figs. 3d and 3e shows an intensive salinity maximum in the boreal summer. Due to the anticlockwise (clockwise) subsurface currents during the boreal winter (summer) driven by the convergences (divergence) in the Banda Sea, the subsurface currents in the eastern passages of the ITF are opposite to those of the surface: southward in the winter and northward in the boreal summer.

4. ITF transport

There are relatively few observational data available to estimate the ITF transport, and hence there is a large uncertainty. The estimation of annual mean

volume varies in the range of 0–30 Sv (Gordon, 2001). The errors in measurement and diagnostic scheme, as well as the significant amplitude of ITF variation on diversified time scales, account for the great uncertainty.

The expendable bathythermograph (XBT) temperature profile along line IX1 [Fremantle-Sunda Straits from (6.8°S, 105.2°E) to (31.7°S, 114.9°E). See the triangles in Fig. 1] is so far the longest time series among the observations related to the ITF. Transport estimated from the line IX1 observation during 1987 to 2001 is employed to verify the annual mean and seasonal variation of the model ITF transport in this section and the interannual variability in the next section.

4.1 *Annual mean*

The simulated and observed transports across line IX1 as well as the primary channels within the Indonesian Seas are listed in Table 1. The annual mean upper layer transport across IX1 (the sum of the upper 700 m geostrophic transport and the Ekman transport calculated from NCEP wind stresses) is 9.6 Sv in the observation. The simulated total transport is 14.5 Sv with 13.2 Sv for the upper 18 levels (about 743 m). Considering the depth of no motion choosen at 700 m in the observation, the integrated current at 700 m along IX1 multiplied by 743 m is subtracted from the upper layer transport of the ITF in LICOM. Thus, the ITF transport relative to the 743-m value is 10.3 Sv, which is much closer to the observation (9.6 Sv) than the previous value. Both the annual mean transports through the Makassar and Ombai Straits are close to the observation. However, the transport is much larger through the Lombok Strait and accordingly much smaller via the Timor Passage, which was also found in other simulations, e.g. the Parallel Ocean Program (POP, Gordon and McClean, 1999).

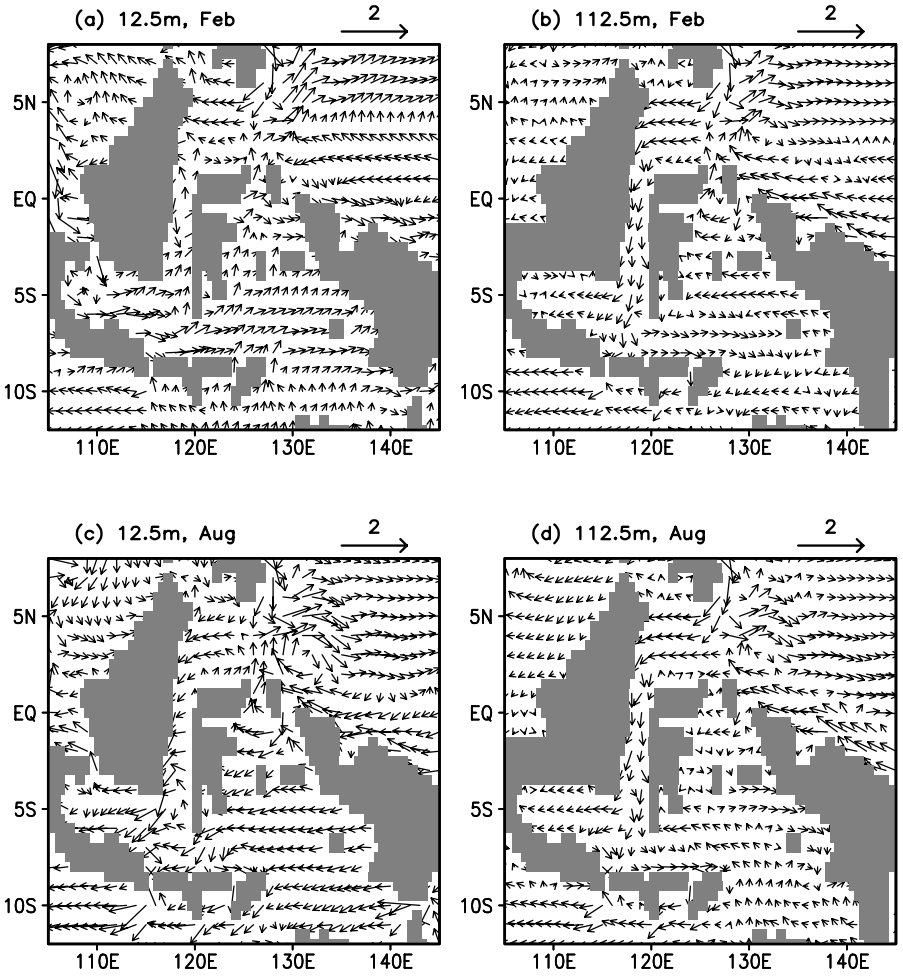

Fig. 4. The simulated velocity vectors at (a, c) 12.5 m and (b, d) 112.5 m. (a) and (b) are for February, (c) and (d) for August. The currents have been divided by the square root of the scalar speed. Units: $m^{1/2}\ s^{-1/2}$.

Table 1. The simulated and observed annual mean transports for the primary channels in the Indonesian Seas (positive is prescribed as from the Pacific to the Indian Ocean). Units: Sv (1 Sv=10^6 m^3 s^{-1}).

	Total	Makassar	Lombok	Ombai	Timor	Torres
LICOM1.0	14.5/10.3[a]	8.0	5.6	6.5	0.7	1.6
Observation	12[1], 9.6[2]	9.3[3]	1.7[4]	5[5]	4.5[6]	0.01[7]

[a] upper layer transport relative to 743 m across line IX1; [1] Godfrey, 1989; [2] Wijffels and Meyers, 2003; [3] Gordon et al., 1999; [4] Murray and Arief, 1988; [5] Molcard et al., 2001; [6] Molcard et al., 1996; [7] Wolanski et al., 1988.

There is a 1.3 Sv transport below 700 m across IX1 in LICOM. The flow must go through both the Timor Passage and the Ombai Strait. Molcard et al. (1996) and Molcard et al. (2001) estimated the transport through these two passages using the data of current meter moorings. The mean transports below 700 m are around 1.3 Sv and 0.6 Sv respectively. Thus, the value of transport in LICOM is smaller than that of the observation, but within its error bar estimations.

4.2 *Seasonal variation*

Confined by the IX1 observation, the following analyses focus on the upper layer (0 to 700 m) transport. In fact, the seasonal variation of the ITF is much stronger in the upper layer than in the deep layers. The variance of the simulated seasonal variation of the ITF is 15.75 Sv^2. Agreeing with the observation, the annual cycle signal is dominant (79% contribution) in the model. Besides, the semi-annual signal is also significant. The monthly mean climatology of the simulated ITF has a maximum (20.4 Sv) in July and the second peak value (11.9 Sv) in January. The minimum (8.2 Sv) occurs in March and the second minimum value (11.35 Sv) in November. The simulated seasonal variation characteristics are consistent with the observation (Fig. 5a, the transport in LICOM is also relative to 743 m as in the observation). The annual signal of the ITF transport is caused by the wind stresses both in the Pacific Ocean and the Indonesian Seas, while the semi-annual signal is mainly generated by the eastward equatorial Kelvin wave driven by the wind stresses in the Indian Ocean (Clarke and Liu, 1993).

The observations show that semi-annual signals are also evident in the transport through the Ombai Strait and the Timor Passage (Molcard et al., 1996; Molcard et al., 2001). As mensioned above, the Lombok Strait provides a major exit for the Indonesian Seas water in the modelling annual mean. Accordingly, the variance of the simulated transport through the Lombok Strait is also of great magnitude. It is worth noting that the simulated semi-annual signal of the ITF transports has a decadal feature. For example, the semi-annual signal is stronger in the 1980s than in other decades. In the Timor Passage, the amplitude of the seasonal variation is small (figure not shown).

Additionally, Figure 5a shows semi-annual signals in the lower layer with the maxima in April and November. Molcard et al. (1996) found the maxima in April and October under 500 m in the Timor Passage during their approximated 1-year observation (their Fig. 10). The maximum transports in the Ombai Strait occurred in April and early November (Molcard et al., 2001). So LICOM simulated a reasonable semi-annual phase under 700 m.

5. Interannual variability of ITF transport

The interannual variability of the ITF transport is related to both the ENSO signal and the "non-ENSO" anomaly from the Indian Ocean (Meyers, 1996; Murtugudde et al., 1998). It is well recognized that the ITF transport tends to be small during El Niño and large during La Niña. The sensitivity experiments conducted by Murtugudde et al. (1998) suggested that the relationship between ITF and the Southern Oscillation Index (SOI) increased from −0.31 to −0.65 when the interannual signal from the Indian Ocean was removed. Based on the simulation driven by European Remote Sensing (ERS) wind from July 1992 through June 1997, Masumoto (2002) found the ITF transport has a closer relationship with the sea surface height anomaly in the eastern Indian Ocean than with ENSO.

The non-ENSO signal from the Indian Ocean detected in Meyers (1996) has an analogous feature in either the pattern or the evolution with the recently discovered Indian Ocean Dipole (IOD) phenomenon (Saji et al., 1999; Webster et al., 1999), i.e., an independent interannual anomaly of the zonal gradient of SST in the Indian Ocean. Hence the index of the IOD mode (DMI) defined by Saji et al. (1999) is used to scale the interannual variability of the Indian Ocean in this study.

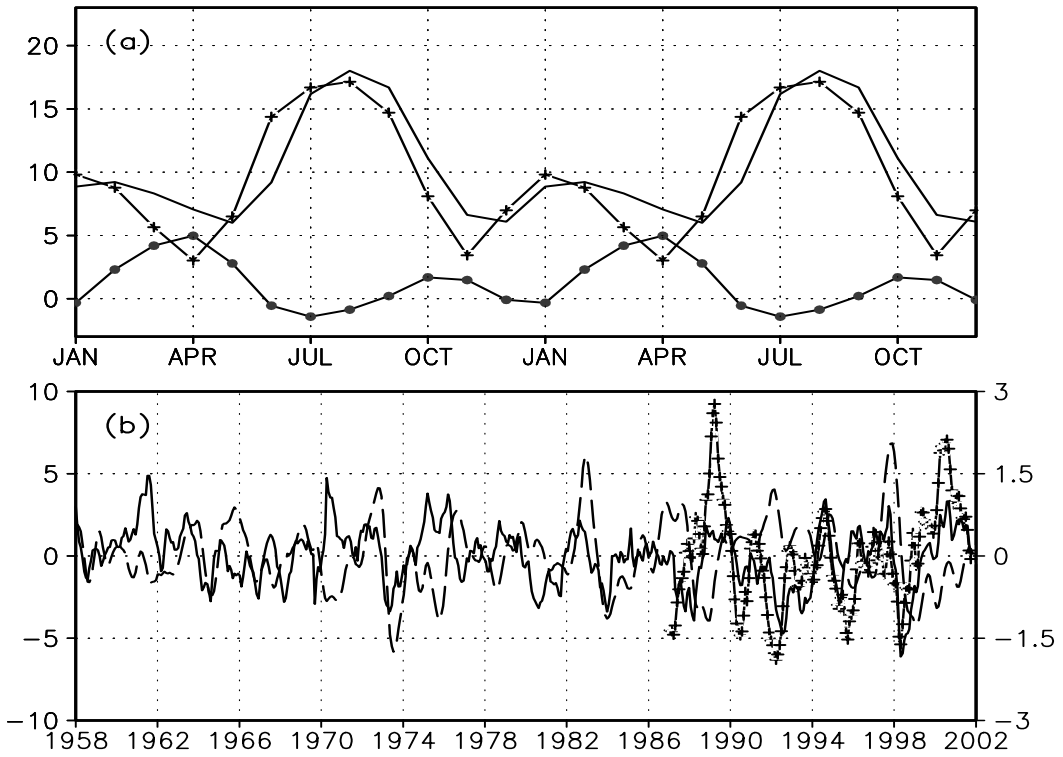

Fig. 5. The simulated (solid) and observed (cross) upper 700 m transport relative to 700 m for the simulation and 743 m for the observation. Units: Sv. (a) monthly mean climatology. The dotted line stands for the transport of the lower layer; (b) the interannual anomalies. The dashed line is the Niño 3.4 index (Units: °C)

5.1 *The interannual evolution of ITF transport, Niño Index, and DMI*

The simulated SST interannual variabilities in the Pacific and Indian Oceans are compared with the observation in Fig. 6. From the Niño 3.4 index (5°S–5°N, 170°–120°W) during 1958 through 2001, LICOM1.0 agrees fairly well with the Global Sea Ice Coverage and Sea Surface Temperature data (GISST, Rayner et al., 1996). The strong warm ENSO events, such as 1982/83, 1986/87, and 1997/98, have especially good agreement with those from the observed in both phase and intensity. For the extreme positive IODs in 1961, 1972, 1982, 1994 and 1997 and negative events in 1964, 1992, 1996 and 1998, the simulated anomalies are reasonable with correct phases but larger amplitudes in most cases. Generally speaking, LICOM1.0 represents the main interannual signal in both the Pacific and Indian Oceans, which provides a basis for the realistic simulation of the interannual variability of ITF.

Compared with the observational transport across line IX1 during 1987 through 2001, the simulated interannual anomaly of ITF has a generally smaller amplitude (Fig. 5b). The main oscillations in the observation, such as the positive anomalies in 1988/89, 1994 and 2000, and the negative anomalies in 1992 and 1998, have been reproduced to some extent. The overall correlation between the ITF transport and Niño 3.4 SST anomaly is significantly negative. The highest correlation is achieved when ITF lags by 4 months (−0.65) and the contemporary correlation is −0.47. The overall correlation between the ITF transport and DMI is also negative, with the highest value of −0.35 for IOD leading by 5 months and −0.13 for zero lag.

5.2 *Impact of ENSO and IOD on ITF transport*

A comprehensive understanding of the relationship of the interannual anomalies between the ITF transport, ENSO, and IOD is beyond the scope of this study. Only the statistical relationship between them is analyzed on the basis of the LICOM1.0 simulation. Now that the simulation of the interannual variabilities of ENSO and IOD has been validated, the investigation is begun from the viewpoint of how the interannual variability of ITF is affected by the anomalies from the Pacific and Indian Oceans.

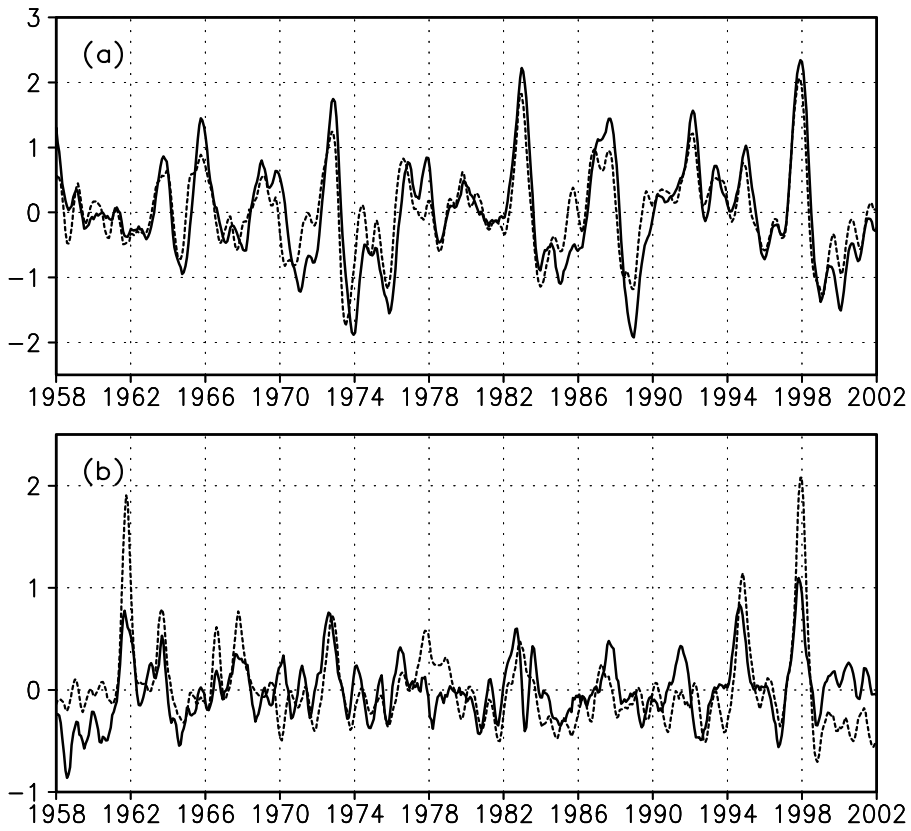

Fig. 6. (a) The Niño 3.4 Index and (b) DMI. The solid line is for GISST and the dashed line is for LICOM1.0. Units: °C.

The correlation pattern between ITF transport and SST anomaly over the tropical Pacific and Indian Ocean (SST leads by 4 months) is exhibited in Fig. 7a. It is found that the pattern of SST anomaly is similar in structure to a cold ENSO event in the Pacific and to a negative IOD event in the Indian Ocean. Due to the cold tongue extended too westward along the equator in LICOM (figure not shown), the correlation coefficients have the same sign across the equatorial Pacific Ocean. This leads to a simulated pattern that is not entirely like a real El Niño one. How can we understand the individual roles played by ENSO and IOD on the ITF transport?

It was pointed out by Wyrtki (1987) that the pressure difference between the western equatorial Pacific and eastern Indian Ocean drives the ITF. Furthermore, Clarke and Liu (1994) advanced that the interannual variability of the ITF transport is highly related to the sea level difference as long as the locations of the two points are correctly chosen. In LICOM1.0, the correlation between ITF transport correlates with the sea level difference [regions of (5°–8°N, 131°–133°E) and (8°–10°S, 111°–113°E)] with a value of 0.50, a result that is not contradictory to the theory of Clarke and Liu (1994). But it should be indicated that the correlation reaches 0.56 when the sea level anomaly at the western Pacific, instead of the sea level difference, is used. The stronger correlation implies that the interannual variation in the Pacific plays a more important role in the interannual variability of the ITF transport in LICOM1.0.

The relationship between ITF transport and the sea surface height (SSH) anomaly in the tropical Pacific and Indian Ocean is shown in Fig. 7b. The sea level anomaly in the western Pacific is closely related to the ENSO event, correlating with a value of −0.63 with the Niño 3.4 Index. This is consistent with the result in section 5.1. The process can be described as a cold ENSO event inducing an east wind anomaly along the tropical Pacific and hence a positive SSH anomaly in the western Pacific, which favors a large ITF transport. The highest correlation coefficient (more than 0.8) can been found off Northwest Australia. That does not contradict the high correlation in the western tropical Pacific. Wijffels and Meyers (2004) suggested that the variation of the Pacific Ocean may affect the SSH in Northwest Australia through the western-propagated Rossby wave and the shoal-following Kelvin wave.

The correlations between ITF transport and the

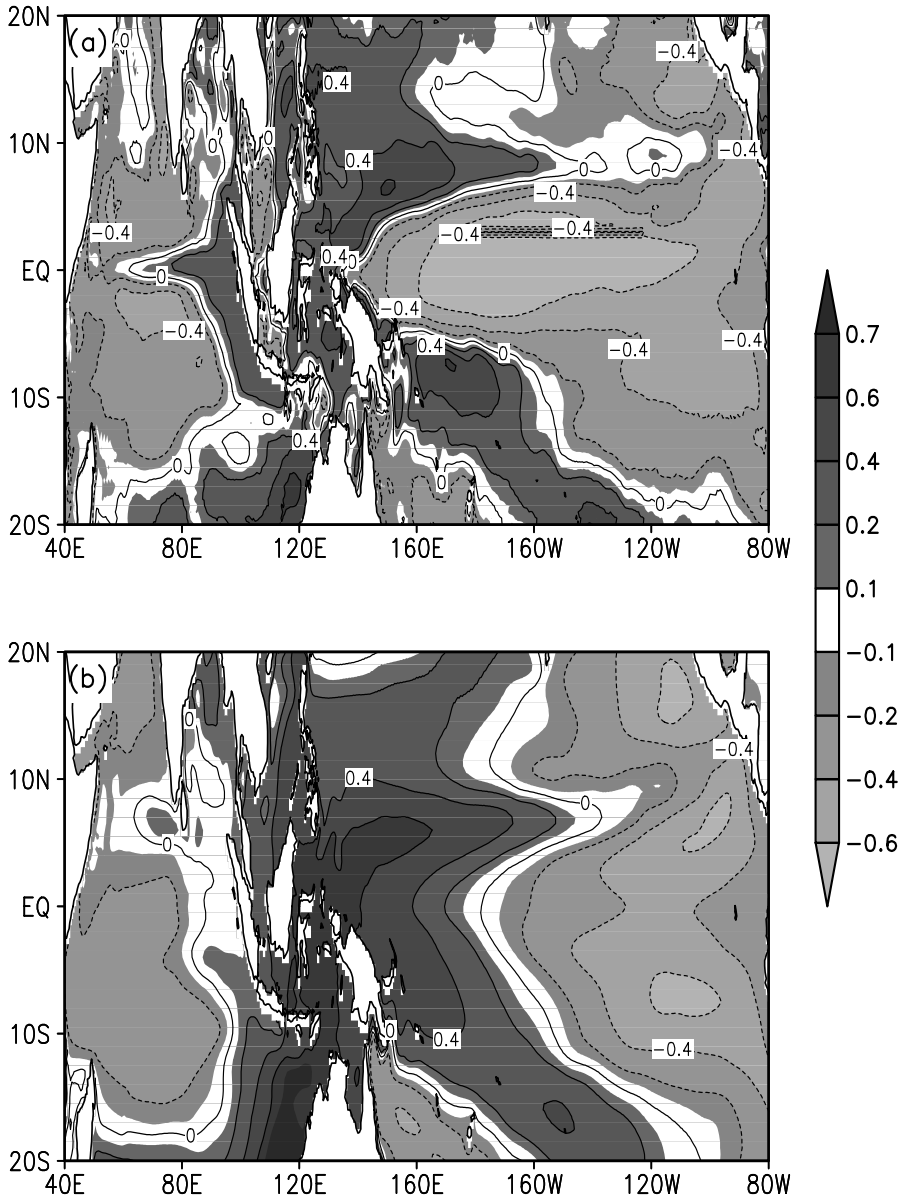

Fig. 7. The correlation of the interannual variability of ITF transport (a) with SST, where the SST is leading by 4 months, and (b) with SSH anomalies, where there is 0 lag time.

SST and SSH anomalies along the Java coast are weak (Fig. 7). It is interesting to notice that the relationship between the ITF and the SST anomaly in the equatorial Indian Ocean has a dipole pattern except for the sign. In terms of Wyrtki's theory, the positive ITF transport anomaly should correspond with a negative SSH anomaly in the eastern Indian Ocean, while the simultaneous relationship between the ITF transport and SSH in the eastern equatorial Indian Ocean is positive in LICOM. The reason is that there is a close relationship between ENSO and IOD. In fact, the relationship between the ITF and interannual variation in the Indian Ocean manifests the dominant influence of the Pacific on the ITF transport. When the ENSO signal is removed from IOD by a simple linear regression, the correlation between IOD and ITF is rather weak (0.07).

The 49-month running correlation shows that the feature of the correlation is not fixed in different periods (Fig. 8). It can be found that there is an obvious decadal variation in the relationship between ITF transport and ENSO whereas the general correlation

is significantly negative. The extent to which the ITF transport is related to IOD is mainly determined by the relationship between IOD and ENSO. Figure 8 confirms that the interannual variability in the Pacific is the leading factor influencing the ITF transport in LICOM1.0.

Although the interannual variability of the ITF transport is generally determined by the signal from the Pacific, the role of the Indian Ocean is important or even dominant for some period. The ITF anomaly in 1994 makes a good case. The mild El Niño implies a weak ITF transport in 1994. In the meantime, the IOD was in an excessive positive phase, with the amplitude of IOD exceeding that of the Niño 3.4 index. In both the observation and LICOM1.0 simulation, the ITF transport is intensified in this year, which reflects the influence of the Indian Ocean on the ITF transport.

Based on the geostrophic current from the observed temperature and salinity, Meyers (1996) pointed out that with an overall strong correlation between ITF and ENSO during 1983 to 1994, there is an exception in May to October 1994. It should be indicated that 1994 is the one and only year of intensified IOD for that observation period. The simulations by Murtugudde et al. (1998) also demonstrate that the abnormal ITF transport in 1994 is derived from the wind anomaly in the Indian Ocean.

6. Concluding remarks

In this study, a quasi-global eddy-permitting oceanic GCM, LICOM1.0, was run with the forcing of ERA40 daily wind stress from 1958 to 2001. The basic climatological mean of the circulation within the Indonesian Seas is reproduced properly. The modelled ITF is reasonable in the aspects of both its water source and major pathways, of which a large volume of transport is through the Makassar Strait. The main defect lies in too much transport through the Lombok Strait and accordingly less through the Timor Passage. The discrepancies in the simulation of salinity profiles in the main straits are caused by the simplicity of the vertical mixing scheme and/or the insufficient resolution, both horizontal and vertical. The seasonal variation of the Indonesian Seas circulation is controlled to a great extent by the transition of the prevailing monsoon.

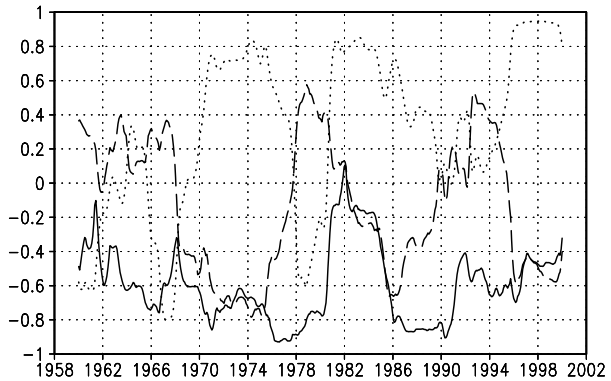

Fig. 8. The 49-month running correlations between ITF transport and Niño 3.4 SST anomaly (solid), ITF transport and IOD SST anomaly (dashed), and Niño 3.4 and IOD SST anomalies (dotted).

The time series of the ITF transport from 1958 to 2001 is obtained and the upper 700 m transport is compared with the observational transport across line IX1 (see Fig. 1). LICOM1.0 simulated a total ITF transport of 14.5 Sv, with 13.2 Sv for the upper 700 m. The annual signal accounts for a large fraction of the seasonal variations, while the semi-annual signal is also clear. The maximums of the ITF transport appear in July and January in turn, and the minimums occur in March and November. Compared with the observation, the simulated annual mean and seasonal cycle of the ITF transport are fairly realistic.

For the 44-year simulation of LICOM1.0, the overall correlation between the interannual anomaly of the ITF transport correlates significantly with the Niño 3.4 index with a value of −0.65. The overall correlation between the ITF and DMI is also negative (−0.35). Further analyses indicate that the interannual variation in the Pacific plays a more important role in the interannual variability of the ITF transport. The relationship between ITF and IOD also reflects the influence of ENSO. Removing the ENSO signal from IOD, the correlation between IOD and ITF is rather weak (0.07). However, the relationship between the ITF transport and the interannual anomalies in the Pacific and Indian Oceans varies with time. During some years, e.g., 1994, the effect of the strong IOD on the ITF transport is more than that from ENSO.

The interannual variabilities of the ITF transport, ENSO and IOD are associated with each other against the backgound of the tropical climate system. Limited by the oceanic GCM, some physical processes involved, especially the air-sea interaction, cannot be interpreted completely in this study. Here, the interannual variability of the ITF transport is merely investigated in the context of ENSO and IOD. Additionally, the ITF thermal and salinity stratifications are modified by the strong mixing within the Indonesian Seas, which is absent in LICOM1.0. Further investigation of both the observation and modelling is needed to understand the interannual variability of the ITF and its relationship with ENSO and IOD.

Acknowledgments. This work was jointly supported by the Chinese Academy of Sciences "Innovation Program" under Grant No. KZCX2-SW-210, the National Key Basic Research of China under Grant No.

G2000078502, and the National Natural Science Foundation of China under Grant Nos. 40233031, 40375030, and 40405017.

REFERENCES

Clarke, A. J., and X. Liu, 1993: Observations and dynamics of semi-annual and annual sea levels near the eastern equatorial Indian Ocean boundary. *J. Phys. Oceanogr.*, **23**, 386–399.

Clarke, A. J., and X. Liu, 1994: Interannual sea level in the Northern and Eastern Indian Ocean. *J. Phys. Oceanogr.*, **24**, 1224–1235.

Fang Guohong, Wei Zhexun, Binghao Choi, Wang Kai, Fang Yue, and Li Wei: 2003: Interbasin freshwater, heat and salt transport through the boundaries of the East and South China Seas from a variable-grid global ocean circulation model. *Science in China* (*Series D*), **46**, 149–161.

Ffield, A., and A. L. Gordon, 1992: Vertical mixing in the Indonesian thermocline. *J. Phys. Oceanogr.*, **22**, 184–195.

Ffield, A., K. Vranes, A. L. Gordon, R. D. Susanto, and S. L. Garzoli, 2000: Temperature variability within Makassar Strait. *Geophys. Res. Lett.*, **27**, 237–240.

Gent, P. R., and J. C. McWilliams, 1990: Isopycnal mixing in ocean circulation models. *J. Phys. Oceanogr.*, **20**, 150–155.

Gibson, J. K., P. Köllberg, S. Uppala, A. Hernandez, A. Nomura, and E. Serrano, 1997: ERA description. ECMWF Reanal. Proj. Rept. Ser. 1, European Centre for Medium-Range Weather Forecasting, Geneva, 72pp.

Godfrey, J. S., 1989: A Sverdrup model of the depth-integrated flow for the world ocean, allowing for island circulations. *Geophys. Astrophys. Fluid Dyn.*, **45**, 89–112.

Godfrey, J. S., 1996: The effect of the Indonesian throughflow on ocean circulation and heat exchange with the atmosphere: A review. *J. Geophys. Res.*, **101**, 12217–12237.

Godfrey, J. S., and Y. Masumoto, 1999: Diagnosing the mean strength of the Indonesian throughflow in an ocean general circulation model. *J. Geophys. Res.*, **104**, 7889–7895.

Gordon, A. L., 2001: Interocean exchange. *Ocean Circulation and Climate: Observation and Modelling the Global Ocean,* Siedler et al., Eds., International Geophysics series 77, Academic Press, New York, 303–314.

Gordon, A. L., and R. Fine, 1996: Pathways of water between the Pacific and Indian Oceans in the Indonesian Seas. *Nature*, **379**, 146–149.

Gordon, A. L., and J. L. McClean, 1999: Thermohaline stratification of the Indonesian Seas: Model and Observations. *J. Phys. Oceanogr.*, **29**, 198–216.

Gordon, A. L., and R. D. Susanto, 1999: Makassar Strait Transport: Initial estimate based on Arlindo results. *Mar. Tech. Soc.*, **32**, 34–45.

Gordon, A. L., R. D. Susanto, and A. L. Ffield, 1999: Throughflow within Makassar Strait. *Geophys. Res. Lett.*, **26**, 3325–3328.

Haney, R. L., 1971: Surface thermal boundary condition for ocean circulation models. *J. Phys. Oceanogr.*, **1**, 241–248.

Hirst, A. C., and J. S. Godfrey, 1993: The role of the Indonesian Throughflow in a global GCM. *J. Phys. Oceanogr.*, **23**, 1057–1086.

Jin Xiangze, Zhang Xuehong, and Zhou Tianjun, 1999: Fundamental framework and experiments of the third generation of IAP/LASG world ocean general circulation model. *Adv. Atmos. Sci.*, **16**, 197–215.

Levitus, S., and T. P. Boyer, 1994: *World Ocean Atlas 1994*. Volume 4: Temperature. NOAA Atlas NESDIS 4, U. S. Department of Commerce, Washington D. C., 117pp.

Levitus, S., R. Burgett, and T. P. Boyer, 1994: *Salinity.* Vol. 3, *World Ocean Atlas 1994*. NOAA Atlas NESDIS 3, U. S. Department of Commerce, Washington D. C., 99pp.

Liu Hailong, 2002: High resolution oceanic general circulation model and the simulation of the upper ocean circulation in the tropical Pacific. Ph.D Dissertation, Graduate School of the Chinese Academy of Sciences, 178pp. (in Chinese)

Liu Hailong, Yu Yongqiang, Li Wei, and Zhang Xuehong, 2004a: Reference manual of LASG/IAP Climate system Ocean Model (LICOM1.0). The special issue of LASG technical report, Beijing, Science Press, 128pp. (in Chinese)

Liu Hailong, Zhang Xuehong, Li Wei, Yu Yongqiang, and Yu Rucong, 2004b: An eddy-permitting oceanic general circulation model and its preliminary evaluations. *Adv. Atmos. Sci.*, **21**, 675–690.

Masumoto, Y., 2002: Effects of interannual variability in the eastern Indian Ocean on the Indonesian Throughflow. *J. Oceanogr.*, **58**, 175–182.

Masumoto, Y., and T. Yamagata, 1996: Seasonal variations of the indonesian throughflow in a general circulation model. *J. Geophys. Res.*, **101**, 12287–12294.

Meyers, G., 1996: Variation of Indonesian throughflow and the El Niño-Southern Oscillation. *J. Geophys. Res.*, **101**, 12255–12263.

Molcard, R., M. Fieux, and A. G. Ilahude, 1996: The Indo-Pacific throughflow in the Timor Passage. *J. Geophys. Res.*, **101**, 12411–12420.

Molcard, R., M. Fieux, and F. Syamsudinb, 2001: The throughflow within Ombai Strait. *Deep-Sea Res.*, **48**, 1237–1253.

Murray, S. P., and D. Arief, 1988: Throughflow into the Indian Ocean through Lombok Strait, January 1985–January 1986. *Nature*, **333**, 444–447.

Murtugudde, R., A. J. Busalacchi, and J. Beauchamp, 1998: Seasonal-to-interannual effects of the Indonesian throughflow on the tropical Indo-Pacific basin. *J. Geophys. Res.*, **103**, 21425–21441.

National Oceanographic Data Center, cited 2004: *World Ocean Atlas 1998*. [Available online at http://www.nodc.noaa.gov/OC5/docwoa98.html]

Pacanowski, R. C., and G. Philander, 1981: Parameterization of vertical mixing in numerical models of the tropical ocean. *J. Phys. Oceanogr.*, **11**, 1442–1451.

Potemra, J. T., 1999: Seasonal variations of upper ocean transport from the Pacific to the indian ocean via indonesian straits. *J. Phys. Oceanogr.*, **25**, 2930–2944.

Potemra, J. T., R. Lukas, and G. T. Mitchum, 1997: Large-scale estimation of transport from the Pacific to the Indian Ocean. *J. Geophys. Res.*, **102**, 27795–27812.

Rayner, N. A., E. B. Horton, D. E. Parker, C. K. Folland, and R. B. Hackett, 1996: Version 2.2 of the Global Sea-Ice and Sea Surface Temperature Data Set 1903–1994. Climate Research Technical Note 74, Meteorological Office, Bracknell, UK., 21pp.

Roeske, F., 2001: An atlas of surface flues based on the ECMWF re-analysis: A climatological dataset to force global ocean general circulation models. Report No.323, Max-Planck-Institut für Meteorologie, Hamburg, 31pp.

Saji, H. N., B. N. Goswami, P. N. Vinayachandran, and T. Yamagata, 1999: A dipole mode in the tropical Indian Ocean. *Nature*, **401**, 360–363.

Schiller, A., J. S. Godfrey, P. C. McIntosh, G. Meyers, and S. E. Wijffels, 1998: Seasonal near-surface dynamics and thermodynamics of the Indian Ocean and Indonesian Throughflow in a Global Ocean General Circulation Model. *J. Phys. Oceanogr.*, **28**, 2228–2312.

Schneider, N., 1998: The Indonesian Throughflow and the global climate system. *J. Climate*, **11**, 676–689.

Webster, P. J., A. Moore, J. Loschinigg, and R. Leben, 1999: Coupled ocean-atmosphere dynamics in the Indian Ocean. *Nature*, **401**, 356–360.

Wijffels, S. E., and G. Meyers, 2003: Fifteen years of XBT measurements in the Indonesian Throughflow. Abstract IUGG General Assembly, Sapporo, Japan.

Wijffels, S. E., and G. Meyers, 2004: An intersection of oceanic waveguides: variability in the Indonesian Throughflow region. *J. Phys. Oceanogr.*, **34**, 1232–1253.

Wolanski, E., E. Rido, and M. Inoue, 1988: Currents through Torres. *J. Phys. Oceanogr.*, **18**, 1535–1545.

Wyrtki, K., 1961: Scientific results of mariane investigation of the South China Sea and the Gulf of Thailand, 1959–1961. *Physical Oceanography of Southeast Asian Water*, Vol. 2, NAGA Rept. 2, Scripps Inst. of Oceanogr., University of Clifania, San Diego, La Jolla, 195pp.

Wyrtki, K., 1987: Indonesian throughflow and the associated pressure gradient. *J. Geophys. Res.*, **92**, 12941–12946.

Zhang Xuehong, Yu Yongqiang, and Liu Hailong, 2003: The development and aplication of the oceanic general circulation model in LASG/IAP, I: The global oceanic general circulation model. *Chinese J. Atmos. Sci.*, **27**, 607–617. (in Chinese)